General Disclaimer

One or more of the Following Statements may affect this Document

- This document has been reproduced from the best copy furnished by the organizational source. It is being released in the interest of making available as much information as possible.

- This document may contain data, which exceeds the sheet parameters. It was furnished in this condition by the organizational source and is the best copy available.

- This document may contain tone-on-tone or color graphs, charts and/or pictures, which have been reproduced in black and white.

- This document is paginated as submitted by the original source.

- Portions of this document are not fully legible due to the historical nature of some of the material. However, it is the best reproduction available from the original submission.

Produced by the NASA Center for Aerospace Information (CASI)

NASA

Technical Memorandum 79586

(NASA-TM-79586) AN EMISSION MECHANISM FOR THE IO-INDEPENDENT JOVIAN DECAMETER RADIATION (NASA) 46 p HC A03/MF A01 CSCL 03B

N78-31027

Unclas

G3/91 29340

An Emission Mechanism for the Io-Independent Jovian Decameter Radiation

Melvyn L. Goldstein and Aharon Eviatar

JULY 1978

National Aeronautics and
Space Administration

Goddard Space Flight Center
Greenbelt, Maryland 20771

TM 79586

AN EMISSION MECHANISM FOR THE IO-INDEPENDENT JOVIAN DECAMETER RADIATION

Melvyn L. Goldstein

NASA/Goddard Space Flight Center
Laboratory for Extraterrestrial Physics

and

Aharon Eviatar

Department of Geophysics and Planetary Sciences
Tel-Aviv University

July 1978

Submitted to *The Astrophysical Journal*

GODDARD SPACE FLIGHT CENTER
Greenbelt, Maryland

CONTENTS

	Page
ABSTRACT	v
I. INTRODUCTION	1
II. THEORY	6
III. APPLICATION TO JUPITER	13
(a) Refraction	15
(b) Source Locations	18
(c) Power Spectrum	22
(d) Emitting Region and Intensity	24
IV. SUMMARY	25
(a) Some Unsolved Problems	27
ACKNOWLEDGMENTS	28
REFERENCES	29

TABLES

Table		Page
1	Comparison of observed and predicted source locations using both the O_4 and JPL multipole magnetic field models	31

ILLUSTRATIONS

Figure		Page
1	Relationship between $\underset{\sim}{v}_g$, $\omega/\underset{\sim}{k}$ and $\underset{\sim}{B}$. Note that when the Appleton-Hartree dispersion relation is used, δ is negative for the extraordinary mode in Band III	32
2	Growth rate versus frequency in Band III. In this calculation m = 2, N = 100, $\zeta = 0.1$ and $u_L = 5.9 \times 10^8$ cm s^{-1}. $\underset{\sim}{B}$ was evaluated at r = 1.06 $R_{\odot}$, $\theta = 54°$ north latitude, and $\lambda_{III} = 201.7°$ with the O_4 model. At that point $\alpha_L = 56°$ compared to $\alpha_E = 2.5°$ at the magnetic equator	33
3	Variation of K_M with ξ for several values of the power-law index, m. N, ζ and u_L as well as r, θ, and λ_{III} are the same as in Figure 2.	34
4	Variation of $\gamma_M/\lvert\Omega_e\rvert$ with ξ for several values of m. Other parameters are the same as in Figure 2.	35
5	Estimated variation of Ψ with frequency. The limit for large angles is determined by refraction. The cutoff toward small angles indicates when convective amplification is small because the wave has moved out of resonance with the electrons	36
6	A plot of K_M and ι versus λ_{III} in the northern (a) and southern (b) hemispheres using the O_4 magnetic field model. Note that K_M is large in the northern hemisphere where ι is small. In the southern hemisphere K_M is large where ι is large. Note that in the southern hemisphere ι is plotted for the 20 MHz source height, while K_M is given for both 20 and 23 MHz.	37
7	Similar to Figure 6, but using the JPL magnetic field model. Note that ι and K_M are not well correlated in either hemisphere.	38
8	Peak radio flux and K_M plotted against frequency. The radio data is taken from Carr and Desch (1976). K_M is the largest value of $K_M(\xi)$ at each frequency. The shape of the K_M curve is a consequence of using a loss-cone distribution to excite DAM.	39

AN EMISSION MECHANISM FOR THE IO-INDEPENDENT JOVIAN DECAMETER RADIATION

Melvyn L. Goldstein
NASA/Goddard Space Flight Center
Laboratory for Extraterrestrial Physics

and

Aharon Eviatar
Department of Geophysics and Planetary Sciences
Tel-Aviv University

ABSTRACT

A theory of the Io-independent decameter radiation is developed. The radiation results from excitation of the electromagnetic loss-cone instability by keV electrons, stably trapped near L = 6. The radiation is excited in Band III of the extraordinary mode. When the effects of refraction are estimated, it is shown that above 10 MHz radiation is beamed into the equatorial plane in a wide, but thin, conical sheet ($\Psi \cong 80°$). When the instability analysis is coupled with one of the octupole models of the Jovian magnetic field, the maximum convective growth of the instability occurs in the directions of the non-Io A, B and C sources. The shape of the peak radio flux frequency spectrum is found to be a consequence of the loss cone shape of the electron distribution function.

AN EMISSION MECHANISM FOR THE IO-INDEPENDENT JOVIAN DECAMETER RADIATION

I. INTRODUCTION

In the preceding paper (Goldstein, Eviatar, and Thieman 1978 – hereafter Paper II) we introduced a model for the Io-independent Jovian decametric emission (DAM) predicated on four basic assumptions: the radiation is produced by stably trapped electrons; it is emitted in the extraordinary mode near the electron gyrofrequency, $|\Omega_e|$; it is beamed into a thin conical sheet; and finally, the occurrence probability of DAM noise storms is associated with the magnitude of the tilt of the emission cone toward the equatorial plane. This last assumption accounted well for the northern hemisphere locations of the Early (B) and Main (A) sources but did not satisfactorily account for the location of the source in the southern hemisphere – the Third source (C). That paper was based solely on geometrical constructions coupled with use of the high order, non-dipolar models of the magnetic field developed following Pioneer 11 encounter with Jupiter (Acuña and Ness 1976, Smith, Davis, and Jones 1976).

The results of Paper II demonstrated that a detailed knowledge of the Jovian magnetic field in the source regions does provide a key to understanding details of the geometric beaming pattern of the Io-independent DAM. However, the model itself was only a framework within which a more complete theory of the decameter radiation could be developed. Ideally, such a theory would provide a physical basis for some of the assumptions used in Paper II; that is the purpose of this communication. This work is motivated by the results of Paper II; and fits within the general framework of that model. The theory is developed from the single assumption that the inner Jovian magnetosphere (L

between 2 and 8) contains a significant number of non-relativistic trapped electrons. This assumption is indirectly supported by electron measurements made on Pioneers 10 and 11. For although instrumentation was not available to detect keV electrons, electrons with energies above several hundred keV were detected throughout the Jovian magnetosphere by Fillius (1976), Van Allen (1976) and McDonald and Trainor (1976). Furthermore, Van Allen (1976) has reported several electron spectra taken between 3 and 20 $R_{♃}$ which extend down to 60 keV. Thus we feel justified in assuming the existence of trapped electrons with keV energies in the inner magnetosphere. Our analysis (and notation) is closely tied to that of Paper II in that extensive use is again made of the octupole models (O_4 and JPL) of Jupiter's magnetic field.

The excitation mechanism upon which this paper is based is the electromagnetic loss-cone instability. We first mentioned this instability in connection with the Io-independent DAM in an earlier paper (Goldstein and Eviatar 1972 – hereafter Paper I). At that time we assumed that the equatorial surface magnetic field could reach 20G, which led to the conclusion that the Io-independent radiation could be generated by electrons in the magnetic equatorial plane -- where the energetic electron densities were greater than elsewhere along a magnetic field line. At the small L values considered ($L \lesssim 2$), the pitch angle anisotropy was large enough to produce substantial growth rates of cyclotron waves.

We now know that the maximum surface magnetic field on Jupiter is about 14G (Smith et al., 1976; Acuña and Ness, 1976), reached only in the northern hemisphere. In the south, the fields do not exceed 10.5G, corresponding to an electron gyrofrequency of only 29 MHz. In view of these observations it is clear that if the non-Io DAM is

amplified cyclotron radiation, it cannot be produced near the equatorial plane, but must be generated at fairly high latitudes and low altitudes (Paper II).

The Pioneer 10 and 11 observations have thus prompted us to reexamine the analysis presented in Paper I, and to propose a somewhat more detailed description of the emission mechanism. This paper also provides an opportunity to clarify some confusion that has arisen in the literature as to the propagation mode of the unstable electromagnetic wave which we had investigated, i.e. whether or not it must tunnel through a stop-zone as it propagates away from the source region.

We pointed out in Paper II that the highest magnetic fields reached by stably trapped electrons correspond to electron gyrofrequencies of no more than 29 MHz – close to the maximum observed frequency of the non-Io DAM (Wilson, Warwick, and Libby 1968). This is consistent with excitation of DAM in the R-X mode very close to either the upper hybrid frequency, ω_{UH} or the cutoff frequency, ω_R, where (Stix 1962)

$$\omega_{UH}^2 = \Omega_e^2 + \omega_{pe}^2$$

and

$$\omega_R = \tfrac{1}{2}|\Omega_e|[1 + (1 + 4\omega_{pe}^2/\Omega_e^2)^{1/2}] \qquad (1)$$

where $\omega_{pe}^2 = \sqrt{4\pi Ne^2/M}$ is the electron plasma frequency. Because the $\omega_{pe}^2 \ll \Omega_e^2$ everywhere in the inner magnetosphere and ionosphere, $|\Omega_e|$, ω_R and ω_{UH} are all nearly equal.

The analysis of the electromagnetic loss-cone instability in Paper I indicated that rapid exponential growth of the linearly unstable waves occurred at frequencies, ω, just below ω_{UH} and just above ω_R (Paper I, Figure 2). Waves excited at frequencies below ω_{UH} propagate in what is called the "Z-mode", or as we prefer, Band II, while the free propagation zone above ω_R will be denoted Band III.

It was pointed out in Paper I that the growth rates of the instability were comparable for waves excited in both Bands II and III. However, waves in Band II cannot escape the Jovian magnetosphere without encountering the stop zone that is reached when the local upper hybrid frequency equals the frequency of the outward propagating wave. For situations in which $\omega_{UH} \cong \omega_R$, a wave in Band II may be able to "tunnel" through the stop zone (Budden 1955), a possibility that was discussed in Paper I and more recently by Smith (1976). Waves excited in Band III have frequencies above the cutoff, and because both the density and field decrease with increasing radius, these waves can freely escape the Jovian environment. The loss-cone instability was shown in Paper I to excite waves in both Bands II and III. We emphasize this point because in several subsequent papers this fact was overlooked (Melrose 1976, Smith 1976) and the electromagnetic loss-cone instability was described as exciting only Band II emission. In this paper, to avoid any further confusion, we will not discuss excitation of Band II emission. The growth rates for emission into the (free-escape) Band III are adequate to explain the Io-independent DAM and tunneling appears to be unnecessary, though it may well make a significant additional contribution.

In the following section we first derive the growth rate for the loss-cone instability at any point along a field line. The trapped electrons are assumed to have a distribution function that is composed of a power-law in velocity together with a loss-cone in pitch angle. Smith's (1976) contention that waves cannot be excited in Band III through resonant interaction is shown to be erroneous for very underdense plasmas. The electrons and waves are able to satisfy the appropriate resonance condition in spite of the fact that the wave phase velocity exceeds the speed of light. The growth rates are calculated at

several frequencies throughout the Jovian magnetosphere, utilizing both the O_4 and JPL spherical harmonic (octupole) models for the magnetic field.

The instability excites electromagnetic radiation above $|\Omega_e|$ in the right circularly polarized extraordinary mode (R-X). The effects of refraction on this mode can be estimated in a straightforward way, as can the total amplification along a ray path. In the absence of nonlinear effects, waves will be amplified until the local value of $|\Omega_e|$ no longer permits the wave-particle resonance condition to be satisfied. At frequencies above 10 MHz, we show that the radiation pattern is confined to a thin conical sheet with half-angle, $\Psi \cong 80\text{-}85°$. At 10 MHz and below, Ψ can be as small as 45-50°.

At frequencies below 20 MHz, the model of Paper II suggested that radiation beamed into a wide conical sheet could intersect the equatorial plane at all central meridian longitudes. Nonetheless, the three decameter sources at those frequencies are still confined to relatively narrow bands of central meridian longitude (CML). The location of the two northern hemisphere sources, non-Io A and B were associated with places where the angle, ι, between the axis of the emission cone and the equatorial plane, was a minimum. A similar suggestion apropos of the Io controlled sources had been made by Dulk (1965) and Schatten and Ness (1971). This idea, which apparently worked so well for sources A and B, gave rather puzzling results when applied in the southern hemisphere. Although the minimum value of ι did occur when one side of the emission cone pointed toward the observed CML of non-Io C, it was the side of the cone pointing toward lower longitudes. In contrast, Io-C is observed when the phase of Io is near 240°, from which one infers that the radiation is beamed into the <u>high</u> longitude side of the emission cone. Thus, the model of Paper II, while correctly locating the northern hemisphere sources, was not consistent with the inferred location of Io-C.

We show in § III that the loss-cone instability growth rates in the northern hemisphere are largest exactly where ι is a minimum, thus providing a natural explanation for the fact that DAM is confined to only those central meridian longitudes where ι is small – elsewhere the growth rates are negligible. By contrast, in the southern hemisphere large growth rates occur near the location of large values of ι – the resulting emission pattern then beams radiation into the Source C longitude range, but now from the same side of the emission cone as had been previously deduced for Io-C. These results obtain only when the O_4 magnetic field model is used. The reasons for this are discussed below.

Several additional features of the observations are discussed in § III, including the shape of the radio intensity versus frequency relation, and the size of the source region. We also present evidence suggesting that the non-Io DAM is produced along the Io flux tube (L = 6).

II. THEORY

We begin this section with a brief review of the theory of the electromagnetic loss-cone instability. The reader is referred to Paper I for more detail. We will be interested, as before, in propagation nearly orthogonal to the background magnetic field, and so we consider wave vectors $\underset{\sim}{k}$ such that $k_\perp/k_\parallel \equiv \tan \xi \gg 1$, where $\parallel$ and $\perp$ are defined with respect to $\underset{\sim}{B}$. When relativistic effects and proton dynamics are ignored, when the bulk of the plasma has a low but finite temperature, and when the number density of the thermal component is much greater than that of the high-energy component, the growth rate of electromagnetic waves is given by (Paper I)

ORIGINAL PAGE IS
OF POOR QUALITY

$$\gamma(\underset{\sim}{k}) = \frac{\pi^2 \omega_{pe}^2 RM}{|k_\parallel|} \int_0^\infty dp_\perp p_\perp^2 \Theta G_1 \Big|_{v_\parallel = v_\parallel^0} \tag{2}$$

where

$$R = -\frac{(\omega^2 - \omega_{UH}^2)^2}{[(\omega^2 - \omega_{UH}^2)^2 + \omega_{pe}^2 \Omega_e^2]}$$

$$\Theta = [J_1(1 - r)/x - J_0]^2$$

$$G_1 = \frac{\partial f_o}{\partial p_\perp} - \frac{k_\parallel}{\omega}\left[v_\parallel \frac{\partial f_o}{\partial p_\perp} - v_\perp \left(\frac{\partial f_o}{\partial p_\parallel}\right)_{p_\parallel = m v_\parallel^0}\right]$$

$$r = |\Omega_e| \omega_{pe}^2 / \omega [\Omega_e^2 - \omega^2 + \omega_{pe}^2]$$

with

$$x = k_\perp v_\perp / \Omega_e$$

and

$$v_\parallel^0 = \frac{(\omega + \Omega_e)}{k_\parallel} \quad .$$

J_n are ordinary Bessel functions of integral order, and f_o is the velocity space distribution function of the energetic electrons normalized so that

$$\int d^3 p\, f_o(\underset{\sim}{p}) = \zeta \tag{3}$$

where ζ is the ratio of the number density of the high-energy electrons to that of the thermal electrons. The rest of the notation follows that of Papers I and II.

The frequency ω is related to $\underset{\sim}{k}$ through the Appleton-Hartree dispersion relation (Stix 1962, p. 38f)

$$n^2 = 1 - \frac{2\nu\omega^2(1-\nu)}{2\omega^2(1-\nu) - \Omega_e^2 \sin^2\zeta - |\Omega_e|\Delta} \tag{4}$$

where

$$\Delta = [\Omega_e^2 \sin^4 \xi + 4\omega^2(1-\nu)^2 \cos^2 \xi]^{1/2} \tag{4}$$

and

$$\nu \equiv \omega_{pe}^2/\omega^2$$

One should note that we will be interested in computing the group velocity, v_g, of the unstable waves. This involves taking derivatives with respect to ξ, and so we cannot make the usual quasi-transverse approximation in which $\Delta \cong |\Omega_e| \sin^2 \xi$.

Before we discuss the functional form of $f_0(\underset{\sim}{p})$ and the evaluation of the growth rate, we want to address the point raised by Smith (1976) that a cyclotron resonance instability cannot excite waves in Band III ($\omega > \omega_R$). In Band III, $\omega/k > c$ (cf. Eq. 4); but on the other hand, to excite the instability $v_{\|}^0 = (\omega + \Omega_e)/k_{\|}$ must be less than c. Even with $k_{\|} \ll k_{\perp}$ the resonance condition can be satisfied if ω is sufficiently close to $|\Omega_e|$. In general this is difficult because ω must also exceed ω_R. However, where $\omega_{pe} \ll |\Omega_e|$ the resonance velocity is approximately given by

$$v_{\|}^0 \sim c \left(\frac{\omega_{pe}}{\Omega_e}\right)^2 \tan \xi \tag{5}$$

The source region of DAM will lie above the Jovian ionosphere where the electron density is completely unknown. However, N will certainly be much less than the maximum ionospheric density ($\sim 10^5 cm^{-3}$) deduced from the Pioneer 11 radio occultation measurement (Fjeldbo et al. 1976). By 3000 km altitude above the cloud tops the analysis of Fjeldbo et al. indicates that $N < 10^3 cm^{-3}$. We consider below the dependence of the loss-cone instability growth rates on values of N ranging from 10 to $10^4 cm^{-3}$. As long as N is $\ll 10^4 cm^{-3}$, excitation of the extraordinary mode in Band III is not a problem, although the bandwidth in ω over which γ is appreciable is very narrow. Note that throughout most of the earth's magnetosphere ω_{pe} is the same order as $|\Omega_e|$, precluding excitation of

cyclotron waves directly into Band III. However, as noted by Smith (1976), in the high-latitude region above the plasmasphere $(\omega_{pe}/\Omega_e) \ll 1$. This is the source location of the Terrestrial Kilometric Radiation (TKR) (Gurnett 1974, Kaiser and Stone 1975).

As in Paper I we choose the electron distribution to be a loss-cone but with a power law velocity dependence. The results of our analysis are not sensitive to the particular functional form chosen for the loss cone and, as before, we assume that relativistic effects can be neglected. Thus

$$\begin{aligned} f_o &= C(1 + p^2/p_L^2)^{-m} \ln(\sin\alpha/\sin\alpha_0) && (\alpha_0 \leq \alpha \leq \pi - \alpha_0) \\ &= 0 && (0 \leq \alpha \leq \alpha_0,\ \pi - \alpha_0 \leq \alpha \leq \pi) \end{aligned} \qquad (6)$$

where α is the pitch angle with respect to the magnetic field, α_0 the loss-cone angle, p_L a parameter that determines the momentum at which this distribution merges into the thermal background, and C is given by

$$C = \frac{2^{m-1}(m-1)!\ \zeta}{\pi^2 p_L^3 [\ln \operatorname{ctn}(\frac{\alpha_0}{2}) - \cos\alpha_0](2m-5)!!}$$

In Equation (6), m is a positive integer greater than one.

We pointed out above, based on the Pioneer 11 models of the Jovian magnetic field, DAM can be produced at frequencies close to ω_R only if the electrons reach the very low altitudes and fairly high latitudes at which the gyrofrequency is in the range of the non-Io emission frequencies (1 - 28 MHz). Using a model of the magnetic field, the mirror altitude and mirror field intensity, the equatorial loss-cone angle, and f_o at the magnetic equator can be determined. Liouville's theorem then prescribes f_o at any magnetic latitude on that field line.

The problem of mapping trapped particle distributions along field lines has been described in detail by Roederer (1970). If we use a subscript "E" to denote quantities

evaluated at the magnetic equator, $f_0(\alpha)$ at some point along the field line is given by

$$f_0(\alpha) = C(1 + \frac{p^2}{p_L^2})^{-m} \ln[(\frac{B_E}{B})^{1/2} \frac{\sin\alpha}{\sin\alpha_E}] \qquad (\alpha_L \leq \alpha \leq \pi - \alpha_L)$$

$$= 0 \qquad (0 \leq \alpha \leq \alpha_L, \pi - \alpha_L \leq \alpha \leq \pi) \qquad (7)$$

where α_L is defined by

$$\sin\alpha_L = (\frac{B}{B_E})^{1/2} \sin\alpha_E$$

In Equation (7) B_E is the magnetic field at the magnetic equatorial plane, while B denotes the intensity of the field at some point along the field line. At that point, α is the pitch-angle and α_L is the local loss-cone angle in the sense that there are no particles at that point with $\alpha < \alpha_L$.

Once a specific representation is chosen for the magnetic field, the growth rate can be evaluated from Equation (2), using Equations (3) and (4) together with Equations (6) and (7).

The Jovian magnetosphere does not provide a homogeneous environment in which a wave can grow at the rate γ. Because of the strong magnetic field gradients, waves initially amplified at the rate γ will soon propagate into regions where the magnetic field and hence γ, have changed. Thus γ will be a function of $\underset{\sim}{r}$. Although the field gradients are large on scales of a Jovian radius, they are generally negligible on a scale of the inverse of the maximum unstable wavenumber, so that the variation in γ with changing $\underset{\sim}{r}$ can be treated by taking the instability as convective, with an unstable wavenumber $K = \gamma/v_g$, where $\underset{\sim}{v}_g = \partial\omega/\partial\underset{\sim}{k}$ is the group velocity of the wave. To evaluate K, v_g must be known as a function of ω and ξ.

ORIGINAL PAGE IS
OF POOR QUALITY

The magnitude of v_g is given by (Stix 1962, p 52f)

$$v_g = \left(\frac{\partial\omega}{\partial k}\right)_\xi \sqrt{1 + \tan^2\delta} \tag{8}$$

where

$$\tan\delta = \frac{-1}{n}\,\partial n/\partial\xi$$

The angle δ is the angle between v_g and $\omega/\underset{\sim}{k}$ (Figure 1). From the dispersion relation (Eq. 4) and the definition of v_g, one finds

$$\frac{1}{c}\left(\frac{\partial\omega}{\partial k}\right)_\xi = \frac{n}{n^2 + \frac{\omega}{2}\frac{\partial}{\partial\omega}n^2}$$

with

$$\frac{\omega}{2}\frac{\partial n^2}{\partial\omega} = \frac{2\nu\left\{-[2(1-\nu) - \frac{\Omega_e^2}{\omega^2}\sin^2\xi + \frac{\Omega_e\Delta}{\omega^2}] + 2(1-\nu)[1 + \frac{\Omega_e}{\Delta}(1-\nu^2)\cos^2\xi]\right\}}{[2(1-\nu) - \frac{\Omega_e^2}{\omega^2}\sin^2\xi + \frac{\Omega_e\Delta}{\omega^2}]^2}$$

and

$$\tan\delta = \frac{2\nu\omega^2(1-\nu)\Omega_e^2\sin\xi\cos\xi}{n^2[2\omega(1-\nu)-\Omega_e^2\sin^2\xi + \Omega_e\Delta]^2}\left[1 - \frac{\Omega_e^2\sin^2\xi - 2\omega^2(1-\nu)^2}{\Omega_e\Delta}\right] \tag{9}$$

For parameters thought typical of the Jovian magnetosphere, δ is generally small ($\lesssim$ 1-2°) and negative, but zero at $\xi = 0$ or $\pi/2$.

As a wave begins to propagate and grow, it is likely to be refracted because of the strong gradients in $\underset{\sim}{B}$. While it is not our intention to perform ray-tracing calculations, we have found that it is quite possible to estimate both where refraction of the extraordinary mode is important, and by how much a wave is likely to be refracted. Such an estimate is crucial for an understanding of just why the decameter radiation is beamed into a wide and thin conical sheet with half angle $\Psi \cong 80°$ and $\Delta\Psi \cong 5°$.

The theory of wave refraction in a cold plasma has been treated by Stix (1962, p. 57–59) and more recently by Smith (1973). We will use only those elements of their analyses most germane for our requirements.

Let $D(\underset{\sim}{k}, \omega, \underset{\sim}{r}) = 0$ be a slow varying function of $\underset{\sim}{r}$. D can be either the dispersion relation or some function of the dispersion relation (Smith uses $D = \omega^2 n^2 - c^2 k^2$).

Then

$$\frac{d\underset{\sim}{k}}{dt} = \frac{\partial D/\partial \underset{\sim}{r}}{\partial D/\partial \omega} \tag{10}$$

For the extraordinary mode

$$\frac{\partial D}{\partial \omega} = 2\omega(n^2 + X\frac{\partial n^2}{\partial X}) \tag{11}$$

$$\frac{\partial D}{\partial \underset{\sim}{r}} \cong \omega^2 \left[-2(X\frac{\partial n^2}{\partial X} + \epsilon\frac{\partial n^2}{\partial \epsilon})\frac{\partial}{\partial \underset{\sim}{r}} \ln B\right] \tag{12}$$

where

$$X = \omega^2/\Omega_e^2$$

$$\epsilon = \omega_{pe}^2/\Omega_e^2$$

The equation for $\partial D/\partial \underset{\sim}{r}$ is valid in regimes where $\epsilon \ll 1$ and gradients in B are larger than gradients in N (Smith 1973). From Equations (10) – (12) we have

$$\frac{d\underset{\sim}{k}}{dt} = v_g \frac{d\underset{\sim}{k}}{ds} \cong -\omega H \frac{\partial \ln B}{\partial \underset{\sim}{r}} \tag{13}$$

with

$$H = \frac{(1-\epsilon/X)[1-\frac{\epsilon}{X}(1-n^2-2\epsilon/X)] - n^2}{2(1-\epsilon/X)-n^2-\frac{\sin^2\xi}{X}}$$

ORIGINAL PAGE IS
OF POOR QUALITY

In the Jovian magnetosphere, the dominant component of the gradient B is along $\underset{\sim}{B}$. Thus,

$$\Delta\xi \cong \frac{\Delta k_{\parallel}}{k} \lesssim \frac{H}{n(v_g/c)} \frac{\Delta B}{B} \tag{14}$$

When using the octupole models of the magnetic field n, v_g, Ω_e and $\Delta B/B$ can be calculated as a wave is convectively amplified. Equation (14) permits estimation of the amount of refraction likely during the wave's growth.

In the following section we utilize the octupole models of the field together with the instability analysis to apply the theory to Jupiter.

III. APPLICATION TO JUPITER

In Paper II, two of the octupole models of the Jovian magnetic field were discussed in some detail. One was the 23 coefficient model constructed by Smith et al. (1976) (denoted JPL) which included three internal (up to octupole) and one external (dipole) term. The second one was the "O_4" model developed by Acuña and Ness (1976) which also had three internal terms, but no external ones. These models differ primarily in the placement of the high field region in the southern hemisphere. This difference necessitates using both field models in the instability analysis.

Before immersing ourselves in detailed calculations of γ and K at various latitudes, longitudes and radii, it is informative to compute γ at one position using various choices for the several parameters (ξ, N, $p_L = Mu_L$, m and ζ).

As an example, consider the growth rate near 20 MHz at System III Longitude λ_{III} = 198°, Θ = 55° north latitude and r = 1.02 $R_{♃}$ (where $R_{♃}$ is one Jovian radius). This is a point on the L = 6 flux-tube. A plot of $\gamma/|\Omega_e|$ versus ω is shown in Figure 2 for Band

III using $\xi = 80°$, $N = 100\ cm^{-3}$, $u_L = 2 \times 10^{-2}$ c (corresponding to 100 eV), m = 3 and $\zeta = 0.1$. As mentioned above, γ is relatively large over only a narrow range of frequencies just above ω_R.

We define the maximum value of $\gamma(\omega)$ as γ_M. $K(\omega)$ is similarly sharply peaked in ω, and we define K_M as its maximum value. (The frequency which defines K_M is nearly equal to that which defines γ_M.) In Figure 3, K_M is plotted against ξ at the same location. Separate curves are shown for m = 2, 3 and 4. As in Figure 2, $u_L = 2 \times 10^{-2}c$, $N = 100\ cm^{-3}$, and the frequency is 20 MHz.

In Figure 3, one can begin to understand both why the conical sheet into which the radiation is beamed is thin and why Ψ is large. At $\xi = 80°$, K_M has dropped to little more than 1/10 of its maximum value near $\xi = 89°$. This strong dependence of K_M on ξ is primarily due to the equally strong dependence of v_g on ξ, which completely dominates the tendency of γ_M to peak at smaller values of ξ (Figure 4). We have also investigated the variation of K_M with u_L, N and ξ. At 20 MHz, with $\xi = 89°$, K_M decreases by a factor of 3 as u_L changes from 3×10^8 cm/s to 1.5×10^9 cm/s. The variation with N is somewhat more complicated. In general K_M increases with increasing N, from 1.4×10^{-7} cm^{-1} with $N = 10\ cm^{-3}$, to $1.1 \times 10^{-6}\ cm^{-1}$ with $N = 100\ cm^{-3}$. As N increases to $10^3\ cm^{-3}$, K_M decreases to $3.3 \times 10^{-7}\ cm^{-1}$ because ω_R is increasing, making the resonance condition more difficult to satisfy. In fact, for densities in the source region much in excess of $10^4\ cm^{-3}$, the loss-cone instability cannot be excited. From Equation (6) one finds that $\gamma \propto \zeta$. For the remainder of the discussion we will take $N = 100\ cm^{-3}$, $u_L = 2 \times 10^{-2}$ c, $\zeta = 0.1$ and m = 3.

(a) Refraction

Before discussing the variation of K_M with longitude, it is necessary to estimate the effects of refraction on the convectively growing wave. As before, we adopt the notation and definitions used in Paper II. Note that longitudes on Jupiter, or in the Jovian magnetosphere, are denoted λ_{III}; where as always, the subscript refers to System III (1965). The observed decameter source locations always refer to the central meridian longitude (CML) of Jupiter at the time of observation. As in Paper II, a distinction is made between the computed direction in the equatorial plane toward which radiation is beamed in the conical sheet and the longitude of the physical location of the emitting region (λ_{III}). The former is denoted $\Lambda_{III}(\pm\mu)$ ($\pm$ designating the side of the cone into which the radiation is beamed). DAM beamed into the direction Λ_{III} will be observable at Earth when the Jovian CML equals Λ_{III}. In the discussion below Ψ refers to the emission cone angle as it might be seen by a remote observer – after the effects of refraction have taken their toll. The angle ξ refers to the cone angle in the source region, and ξ_a will be used, when needed, to single out the initial value of ξ at the apex of the emission cone before any refraction has occurred. Thus, a ray might start off with $\xi_a = 89°$, be refracted to $\xi = 85°$ in the middle of the source region, and finally emerge with $\Psi = 80°$.

In Section II we derived a formula (Eq. 14) useful for estimating the amount of refraction experienced by a wave propagating through source region. Equation (14) then provides an indication of the ray path. Along the ray path, beginning at the apex of the emission cone, the quantity

$$A^{\pm}(S) \equiv 2 \int_0^S ds' K_M(s') \tag{15}$$

can be computed, at least approximately. In Equation (15), + and - signs refer to the two directions toward which the emission cone intersects the equatorial plane (i.e. $\Lambda_{III}(+\mu)$ or $\Lambda_{III}(-\mu)$). At S, B(s) has changed from its value at s = 0 (the apex of the cone) so that $\gamma(s = S) \cong 0$. $A^{\pm}$ is roughly proportional to the logarithm of the intensity. In estimating $A^{\pm}$ we have not included any nonlinear saturation processes. In fact, for some choices of parameters, it is not clear that nonlinear processes are required because the gradients of the magnetic field seem adequate to limit the convective growth to that demanded by the observations. We will return to this point below.

Because δ is generally a small angle, the important parameter in estimating the refraction is ξ_a. We have seen in Figure 3 that for $\xi_a << 80°$, K_M is small. In addition $v_g \cong c$ and not only is $A^{\pm}$ small, but refraction is negligible. Using Equations (14) and (15) we found that when ξ_a ranged from 85° to 89°, refraction would result in the ray leaving the source region with Ψ between 80–85°. Recall from Paper II that $\Psi \cong 80°$ was required to properly locate the non-Io A and B sources in the northern hemisphere.

So far only the results at 20 MHz have been discussed. The balance between refraction and efficient growth is a function of frequency. At the highest frequencies, near 27 MHz, even $\xi \cong 80°$ is too small for convective growth because the very strong field gradients rapidly destroy the wave-particle resonance. At the other end of the spectrum, $f \cong 10$ MHz and below, the weak gradients in B permit substantial growth at all $\xi \gtrsim 50°$. Below $\xi \cong 50°$, our formula for γ becomes invalid.

This effect can be illustrated, if only approximately, by using Equations (14) and (15) to find the likely range of Ψ with which an amplified wave will leave the source region. The results at 27, 20, 16 and 10 MHz are shown in Figure 5. Values of Ψ larger than

about 85° are prohibited by refraction, while the lower limit at each frequency indicates where the convective amplification is small because changes in B have moved the particles out of resonance.

The exact relationship between the observations and the results discussed above is not completely clear, for the observations sum over the entire source region. However the general trend of the theory is that at high frequencies ($f \gtrsim 20$ MHz), radiation is preferentially excited into a very thin sheet ($\Delta\Psi \cong 3°$) with $\Psi \cong 85°$; between 16 and 20 MHz, $\Delta\Psi \lesssim 10°$ and typically $\Psi \cong 80°$. At still lower frequencies ($f \cong 10$ MHz) Ψ can range from 45–85°. In Paper II, we found that such a shift of Ψ with frequency could account for the observed single peak in the occurrence probability at 200° CML at 10 MHz (Thieman and Smith 1978).

These calculations could be improved by simultaneously solving Equations (10) and (15) along the ray path. The effects of refraction would then be rather precisely determined, at least within the context of the field and density models employed. However, there are several complications with that approach, for as the ray is refracted, it moves away from the equatorial plane. Of course, some other ray not originally intersecting that plane will be refracted into it, but this means that to follow a ray toward a remote observer in the equatorial plane, one must actually move backwards along the ray path from the observer to the point where K_M at that frequency is maximum. Such a calculation is well beyond the scope of the present analysis, which we believe suffices in providing reasonable estimates of refraction.

(b) Source Locations

In this section we will use the results of Paper II along with estimates of $K_M(\lambda_{III})$ to find the predicted source location of DAM as seen by a distant observer in the Jovian equatorial plane. The numerical results discussed thus far have been evaluated at L = 6, the Io flux tube. We have also computed $K_M(\xi_a)$ at L = 2, 3, 4 and 5. The range in ξ_a over which K_M is large does not vary with L, remaining between 80° and 89.9° (f > 10 MHz). Furthermore, numerical estimates of both the amount of refraction and amplification of the ray again indicate that it will be refracted until $\xi \cong 80°$, and that $\xi \lesssim 80°$ is precluded because gradients in B destroy the wave-particle resonance. Paradoxically, because these features of the analysis do not vary significantly with L, one can argue that the source region is, in fact, located near L = 6. First of all, by L = 2 the growth rates have become too small to account for the observed fluxes, but more importantly; we noted in Paper II that if the DAM source were inside L = 6, the geometrical model would better fit the locations of the Main and Early sources if Ψ (or ξ) was no larger than 60°. However, as we have demonstrated above, at frequencies greater than 10 MHz, gradients in B destroy the resonance if $\xi < 80°$. Furthermore, we found that refraction is not likely to be strong enough to bend a ray by more than 10° at any L value. Thus, the results of the present analysis, taken together with the results of Paper II, suggest that the Io-independent sources are located near the Io flux tube. (Note that in neither Paper II, nor in the present analysis have L values greater than six been considered.) Exactly how Io might influence the excitation of the "Io-independent" DAM will not be considered here. In the remainder of this subsection, we assume that the sources are located near L = 6 and use the O_4 and JPL field models to determine the CML of the decameter sources.

In Figure 6 we show $K_M(\xi_a = 89°)$ at 20 MHz as a function of λ_{III} using the O_4 magnetic field model. The results are shown for the northern hemisphere. For comparison, ι is also plotted. Note that the locations of large K_M correspond to regions of small ι. Thus we have a clear physical explanation for the relationship discussed in Paper II between ι and source location, viz., in the northern hemisphere the loss-cone instability is strongest precisely where the axis of the emission cone has the greatest tilt toward the equatorial plane.

From Figure 6a K_M is largest in the region $165° \lesssim \lambda_{III} \lesssim 210°$. With $\Psi \cong 80°$, radiation from this region will be beamed into the equatorial plane from one side of the cone in the direction

$$95° \lesssim \Lambda_{III}(-\mu) \lesssim 170°$$

From the other side of the cone radiation will be beamed toward $240° \lesssim \Lambda_{III}(+\mu) \lesssim 315°$. Over the part of the region where Λ_{III} exceeds 270° the radiation is actually directed toward the cloud tops because of the large tilt of the cone axis out of the meridional plane. Therefore between $\Lambda_{III}(+\mu) = 270°-315°$ radiation may be absorbed or reflected by the planet. We will make no allowance for this, and take the source region to be

$$240° \lesssim \Lambda_{III}(+\mu) \lesssim 315°$$

These ranges should be compared with the observed locations of the non-Io B and A sources (Carr and Desch 1976 – this range refers to all frequencies between 11 and 28 MHz, at 20 MHz the source sizes are smaller)

$$95° \lesssim \Lambda_{III} \lesssim 195° \qquad \text{Non-Io B}$$

$$195° \lesssim \Lambda_{III} \lesssim 285° \qquad \text{Non-Io A}$$

In the southern hemisphere a similar calculation produces quite different results (Figure 6b). Now K_M is relatively small where ι is a minimum, and large amplification rates are found where the emission cone is tilted away from the equatorial plane. The largest growth rates are found near λ_{III} between 220°-260°. The resulting beaming pattern, again assuming $\Psi \cong 80°$, results in apparent source locations of

$$290° \lesssim \Lambda_{III}(+\mu) \lesssim 330°$$

and

$$155° \lesssim \Lambda_{III}(-\mu) \lesssim 195°$$

while non-Io C is found between the central meridian longitudes

$$285° \lesssim \Lambda_{III} \lesssim 5°$$

From estimates of $A^{\pm}$ in these regions we found a tendency for A^+ to be significantly larger than A^-. In Paper II, we showed that where ι was small, the emission cone intersected the equatorial plane so that $\Lambda_{III}(-\mu)$ corresponded to Source C. Now we find that the largest growth rates are found where the $+\mu$ side of the cone corresponds to Source C. This is an encouraging development because it places the Io-independent source close to the location of the Io-controlled one. From the Io-phase versus CML relationship, it is known that Io-C is emitted from the high longitude (i.e. $+\mu$) side of the emission cone. That A^+ is larger than A^- is consistent with the fact that no non-Io left polarized source is observed in the range 155-180° CML.

Non-Io C is only observed at frequencies below about 23 MHz. At 23 MHz K_M has decreased substantially from its values at 20 MHz (Figure 6b). There is only one area ($\lambda_{III} \cong 235°$) where K_M is not completely negligible. Again $\Lambda_{III}(+\mu) \cong 300°$ (Source C), and $A^+ > A^-$. Furthermore, in the region around $\lambda_{III} \cong 50°$, where ι is a minimum,

$K_M \cong 0$. This tends to confirm our association of the emitting region of Source C with $\lambda_{III} \cong 235°$ in the southern hemisphere.

A similar analysis using the JPL magnetic field model yields somewhat different results. As noted in Paper II, this model differs substantially from O_4 in that the maximum southern hemisphere fields are found 100° further west than the corresponding maximum in the O_4 model (cf. Figures 1 and 2 of Paper II). This coupled with our basic assumption that the radiation is produced by trapped electrons results in rather different longitudes for the largest values of K_M. In the northern hemisphere (Figure 7a), K_M and ι are no longer in phase. In fact, at the longitude of smallest ι, K_M is near its minimum.

In the northern hemisphere K_M is largest between $220° \lesssim \lambda_{III} \lesssim 60°$ – a range of some 200°. The resulting emission pattern is beamed into the equatorial plane from

$$180° \lesssim \Lambda_{III}(-\mu) \lesssim 300°$$

and

$$330° \lesssim \Lambda_{III}(+\mu) \lesssim 80°$$

where $\Psi = 80°$. These results are not encouraging, for they do not approximate the known source locations of the Early and Main Sources.

In the southern hemisphere K_M is large from $\lambda_{III} \cong 270°$ to $\lambda_{III} \cong 20°$. Radiation beamed into an 80° cone will then be seen from the central meridian longitude ranges

$$215° \lesssim \Lambda_{III}(-\mu) \lesssim 310°$$

and

$$350° \lesssim \Lambda_{III}(+\mu) \lesssim 95°$$

Although these do not appear to include the Source C region, we find evidence from evaluating $A^{\pm}$ that significant amplification does occur when $\Lambda_{III} \cong 300\text{–}340°$. Curiously, both A^+ and A^- are large within that range.

Although the O_4 field model apparently provides a clearer explanation of the source locations, at least within the context of the assumptions of this theory, one should keep in mind that both models are derived from similar data sets. In both cases the data sets are insufficient to precisely determine the Jovian magnetic field everywhere within the magnetosphere. In constructing the O_4 and JPL models, the limited magnetic field measurements were apparently analyzed using somewhat different analytical techniques. If one could ascribe "error bars" to the set of models derivable from the Pioneer 11 data, the O_4 and JPL models might then be representative ones – both equally valid to the precision of the data and limited spacecraft trajectory. Furthermore, our use of these models, especially in this paper, has tended to amplify the differences between them. Therefore one should probably take the view that it is encouraging that within the group of allowable magnetic field models, there appears to be at least one that is consistent with this theory of DAM. In addition, it is clear that detailed predictions of the source locations of DAM sources are very sensitive to the local structure of the magnetic field. Only better measurements will resolve these differences, and allow closer comparisons between theory and experiment.

(c) Power Spectrum

One aspect of the DAM observations not yet addressed is the way in which intensity varies with frequency. In Figure 8 the log of the peak intensity of DAM, F, is plotted against frequency. The curve, taken from Carr and Desch (1976), includes radiation from both Io-controlled and Io-independent sources. However, in his thesis Desch (1976) found that when only the non-Io-controlled component is considered, the intensity spectrum has the same shape, with reduced intensities. Only the shape of the curve concerns us in this section.

As long as the size of the source region is approximately constant at all frequencies, the logarithm of the intensity should be roughly proportional to the convective growth rate, K_M. But K_M at a specific frequency is also a function of ξ. We have seen that at 20 MHz $K_M(\xi)$ is largest at $\xi \cong 89.5°$ (Figure 3). As the frequency decreases so does the angle ξ at which K_M is largest. This decrease is rather small until f falls below 10 MHz. From 10 to 2.5 MHz the ξ of maximum K_M decreases from 89° to 75°. Even smaller values are found below 2.5 MHz, but because the growth rate calculation assumes $k_{\parallel}/k_{\perp} \ll 1$ ($\xi \gg 45°$) the resulting values for K_M are unreliable. The largest $K_M(\xi)$ is also plotted in Figure 8, the dot–dashed line below 2.5 MHz indicating the frequency range in which ξ is less than 75°. [The calculation of K_M was done using the O_4 model along the northern hemisphere field line crossing the equatorial plane at $\lambda_{III} = 230°$.]

Because the relative scales between the two quantities were arbitrarily chosen, the significant features of the curves are that they both peak near the same frequency (f $\cong$ 10 MHz for K_M, and f $\cong$ 8 MHz for F), and they both decrease to very small values at 1 and 27 MHz.

The shape of the K_M curve is primarily dictated by the assumption that the instability is excited by free energy in the particle's loss–cone distribution. At the lowest frequencies, the local loss–cone angle is small ($\alpha_L \cong 15°$) so there is little velocity–space anisotropy to drive the instability. Conversely, at the highest frequencies, α_L is large ($\alpha_L \cong 75°$ at 27 MHz) but nearly all electrons have mirrored, leaving too few particles to excite a strong instability. Somewhere in between these two competing effects convolve to produce the maximum instability. The shape of the observed peak flux curve is evidence that the particles' loss–cone angle plays an important role in exciting DAM.

(d) Emitting Region and Intensity

Jovian noise storms have been observed using very long baseline interferometer (VLBI) radio antenna systems in an attempt to measure the extent of the emitting region. Observations have been confined to looking at the Io-B source at 34 and 18 MHz. At 34 MHz, the observed noise storms were S-bursts (Dulk 1970), while Lynch et al. (1972), observing at 18 MHz, analyzed an L-burst. In both cases, the sources, assuming they were incoherent, were unresolved, indicating linear dimensions less than 400 km. To our knowledge, no interferometry has been done on non-Io sources. For the purposes of this discussion, then, we assume that the non-Io sources also have linear dimensions of several hundred kilometers. Within such a distance the radiation must be amplified from noise to a peak flux of nearly 10^6 Jy* (at 20 MHz). That noise level can be estimated by assuming that electrons participating in the instability amplify their own incoherent cyclotron radiation. At earth, the noise level would be (Jackson 1962)

$$F_o = \frac{\zeta N P v_g}{\Delta f} \left(\frac{\Delta x}{r}\right)^2 \tag{16}$$

where $(\Delta x)^2$ is the area of the emitting region (taken to be 1.6×10^5 km^2), Δf is the receiver bandwidth and

$$P = \frac{2}{3} \frac{e^2 v^2}{c^3} \Omega_e^2 \tag{17}$$

With $\Delta x \cong (400$ km), $F_o \cong 1$ Jy, which implies that $A^{\pm}$ must be about 16. Such amplifications are rather easily achieved at the longitudes characteristic of the peak values of K_M. Furthermore, these amplifications typically result from traversing a path length of

*(Jy $\equiv 10^{-26}$ W m^{-2} Hz^{-1}

a few hundred kilometers. Thus the growth rates we have computed appear fully capable of amplifying incoherent cyclotron radiation to the peak observed intensities within dimensions less than, or of order, the upper limits of the source size. The time necessary to reach these intensities is less than one second.

That the excited waves convect out of resonance after amplifying by the approximate amount required to account for the observed intensities suggests that nonlinear processes may not always be important in limiting the growth of the waves. Also, because we lack sufficiently detailed information about the plasma environment in the emitting region, it is difficult to suggest mechanisms whereby nonlinear processes, be they wave-particle or wave-wave, limit the growth of the instability.

There is, however, one effect that will tend to inhibit amplifications much in excess of the e^{16} estimated above. Because the growth rates are so sharply peaked in frequency, electrons will become phase coherent or magnetically trapped by the wave if the amplitude becomes too large. Equations (16) and (17) can be used to estimate the noise level of the magnetic field fluctuations. At 20 MHz we find that $\delta B \cong 10^{-11}$ G, and the magnetic trapping time, τ is of the order

$$\tau \sim \left(\frac{mc}{k_{\parallel} e v_{\perp} \delta B}\right)^{1/2} \gtrsim 0.1\,\mathrm{s} \tag{18}$$

With $\gamma \sim 10^{+2}\ \mathrm{s}^{-1}$ there is time for 10 or so exponentiations before τ exceeds γ^{-1}, tending to inhibit further wave growth.

IV. SUMMARY

The theory presented here has evolved from one basic assumption: the inner Jovian magnetosphere ($L \sim 6$) is populated by keV electrons stably trapped in Jupiter's magnetic

field. From this, we have shown that the electron distribution is unstable to the electromagnetic loss-cone instability, producing radiation in the R-X mode near the local electron gyrofrequency. Significant amplification is expected from 1 MHz to 28 MHz, with a peak near 10 MHz, which corresponds very closely to the observed frequency range and spectral shape of the Io-independent decameter spectrum. The competition between refraction and convective growth of the radiation in regions of strong radial gradients in B limits the radiation pattern at frequencies above 10 MHz to a wide, but thin, conical sheet with $\Psi = 80°-85°$. At altitudes where the gyrofrequency is less than or equal to 10 MHz, the gradients in B are relatively small so that significant wave growth is possible over a much wider range of cone angles: $50° \lesssim \Psi \lesssim 80°$.

Thieman and Smith (1978), showed that by 10 MHz sources A and B appear to have been replaced by a single source near $\Lambda_{III} \cong 200°$. We argued in Paper II that the effect would result from a decrease in Ψ from 80° above 10 MHz to $\Psi \cong 40°$ at 10 MHz. Efficient wave excitation at frequencies below 10 MHz with Ψ as small as 50° or less is certainly suggested by our results.

Because of the very non-dipolar nature of the Jovian magnetic field, large variations of K_M with λ_{III} were found which enabled us to predict the location of the DAM sources. Those results are summarized in Table 1. Radiation excited where K_M is largest is beamed into the equatorial plane from either side of the wide emission cone ($\Psi = 80°$). From the northern hemisphere (O_4 model), the apparent source locations agree quite well with the known locations of non-Io A and B to within 30°. Using the JPL model results in a poorer fit. From the southern hemisphere both field models suggest a DAM source consistent with the location of non-Io C. In addition the O_4 model indicates the possible

existence of a weak left polarized source near 155°-180° CML. Such a source, if it exists, should be observable by the Voyager spacecraft. Furthermore we found that the theory requires that the Io-independent DAM be excited on flux tubes with $L \gtrsim 6$.

In Paper II we noted that the geometry of the northern hemisphere sources could be understood by associating the source locations with small values of ι. This postulate has a natural explanation when the O_4 field model is used, for then ι is smallest where K_M is largest (Figure 6a). That the postulate failed to account for the location of source C can be understood because in the southern hemisphere small values of C are no longer correlated with large K_M, and the source location for non-Io is more naturally associated with the large values of K_M (Figure 6b).

Because the time scales for exponential growth are of the order 10^{-2} s, S-bursts cannot be excited by this mechanism, but S-bursts are a unique feature of the Io-controlled sources; so this is not a limitation of the theory. The growth rates we have found are also consistent with constraints placed on the source size by VLBI observations, assuming those results can be extrapolated to the Io-independent sources; i.e., the observed peak fluxes are achieved after convective growth over distances of 400 km or less. At 20 MHz, larger source sizes are unlikely because the gradients in B will move a wave out of resonance by the time it has travelled 400 km.

(a) Some Unsolved Problems

The theory presented here appears capable of explaining many features of decameter phenomenology. However, there are aspects of the observations that we have not addressed. Chief among them is the well known asymmetry in the occurrence probabilities of the non-Io A and B sources. Even in the Desch et al. (1975) study at 26.3 MHz, where

non-Io B had an occurrence probability twice that of non-Io A, the intensities of the two sources differed greatly (B was less intense than A). The explanation of this effect may require a combination of better magnetic field models and more precise ray-tracing calculations than used here. Our estimates of $A^{\pm}$ (Eq. 15) did suggest differences between A^{+} and A^{-}, but none sufficiently striking as to provide a clear explanation for the observed differences between non-Io A and B.

Another problem not discussed is the question of the source of the trapped electrons. The instability we considered will stabilize and turn itself off at any particular location after several seconds. Additional bursts from that area would require a fresh supply of electrons. If the L = 6 flux tube is the source of the radiation, then Io could perhaps indirectly provide the necessary particles. Alternatively, the suggestion has been made that the occurrence of Io-independent emission is correlated with fluctuations in solar wind parameters (v., e.g. Terasawa, Maezawa, and Machida 1978), suggesting the solar wind as the possible source of the electrons. This brings us to the question of the relationship between this mechanism for exciting the Io-independent DAM and theories of the Io-controlled component. It is a question we hope to address in future research.

ACKNOWLEDGMENTS

The authors would like to express their warm appreciation for the continued encouragement of Mr. Joseph Alexander and Drs. Norman Ness, Leonard Burlaga and Keith Ogilvie. The comments and contributions of Drs. James Thieman, Michael Desch and Alain Roux are greatfully acknowledged. Mr. Mark Silverstein is thanked for his assistance with some of the numerical analysis. One of us (A. E.) acknowledges the support provided by the Department of Physics and Astronomy of the University of Maryland and the

Laboratory for Extraterrestrial Physics of the Goddard Space Flight Center during the summer of 1977, when this work was begun.

REFERENCES

Acuña, M. H., and Ness, N. F. 1976, in Jupiter, ed. T. Gehrels (Tucson: University of Arizona Press), p. 830.

Budden, K. G. 1955, in Physics of the Ionosphere: Report of Phys. Soc. Conf. Cavendish Lab., Phys. Soc., London, p. 320.

Carr, T. D., and Desch, M. D. 1976, in Jupiter, loc. cit., p. 693.

Desch, M. D. 1976, Ph. D. Thesis, University of Florida, Gainsville, Florida.

Desch, M. D., Carr, T. D., and Levy, J. 1975, Icarus, 25, 12.

Dulk, G. A. 1965, Science, 148, 1585.

Dulk, G. A. 1970, Ap. J., 159, 671.

Fillius, W. 1976, in Jupiter loc. cit., p. 896.

Fjeldbo, G., Kliore, A., Seidel, B., Sweetnam, D., and Woiceshyn, P. 1976, ibid., p. 238.

Goldstein, M. L., and Eviatar, A. 1972, Ap. J., 175, 275.

Goldstein, M. L., Eviatar, A., and Thieman, J. 1978, NASA TM 79537.

Gurnett, D. A. 1974, J. Geophys. Res., 79, 4227.

Jackson, J. D. 1962, Classical Electrodynamics (New York: John Wiley), p. 471.

Kaiser, M. L., and Stone, R. G. 1975, Science, 189, 285.

Lynch, M. A., Carr, T. D., May, J., Block, W. F., Robinson, V. M., and Six, N. F. 1972, Astrophys. Letters, 10, 153.

McDonald, F. B., and Trainor, J. H. 1976, in Jupiter, loc. cit., p. 961.

Melrose, D. B. 1976, Ap. J., 207, 651.

Roederer, J. G. 1970, Dynamics of Geomagnetically Trapped Radiation (New York: Springer-Verlag), Chapter 4.

Schatten, K. H., and Ness, N. F. 1971, Ap. J., 165, 621.

Smith, E. J., Davis, Jr., L., and Jones, D. E. 1976, in Jupiter, loc. cit., p. 788.

Smith, R. A. 1973, Ph. D. Thesis, University of Maryland, College Park, Maryland.

Smith, R. A. 1976, in Jupiter, loc. cit., p. 1146.

Smith, R. A. 1976, Astrophys. Letters, 17, 167.

Stix, T. H. 1962, The Theory of Plasma Waves (New York: McGraw Hill).

Teresawa, T., Maezawa, K., Machida, S., 1978, Nature, 273, 131.

Thieman, J. R. and Smith, A. G. 1978, preprint.

Van Allen, J. A. 1976, in Jupiter, loc. cit., p. 928.

Wilson, R. G., Warwick, J. W., and Libby, W. F. 1968, Nature, 220, 1215.

Table 1

Comparison of Observed and Predicted Source Locations Using Both the O_4 and JPL Multipole Magnetic Field Models

Observed Source Locations (after Carr and Desch 1976)	Polarization R = Right, L = Left		f = 20 MHz, $\Psi \sim 80°$, L = 6			
			O_4		JPL	
	Observed	Predicted	Source Locations	λ_{III} of Emitting Region	Source Locations	λ_{III} of Emitting Region
Non-Io A 195°-285° (11-28 MHz)	R	R	$\Lambda_{III}(+\mu)$ 240°-315°	165°-210°	$\Lambda_{III}(+\mu)$ 330°-80°	220°-60°
Non-Io B 95°-195° (11-26 MHz)	R	R	$\Lambda_{III}(-\mu)$ 95°-170°		$\Lambda_{III}(-\mu)$ 180°-300°	
Non-Io C 285°-5° (11-22 MHz)	L	L	$\Lambda_{III}(+\mu)$ 290°-330°	200°-260°	$\Lambda_{III}(+\mu)$ 350°-95°†	270°-20°
		L	$\Lambda_{III}(-\mu)$ 155°-195°*		$\Lambda_{III}(-\mu)$ 215°-310°†	

*Estimates of A^- indicate weak amplification.
†Estimates of A^+ and A^- indicate large amplification in the 300-340° longitude range.

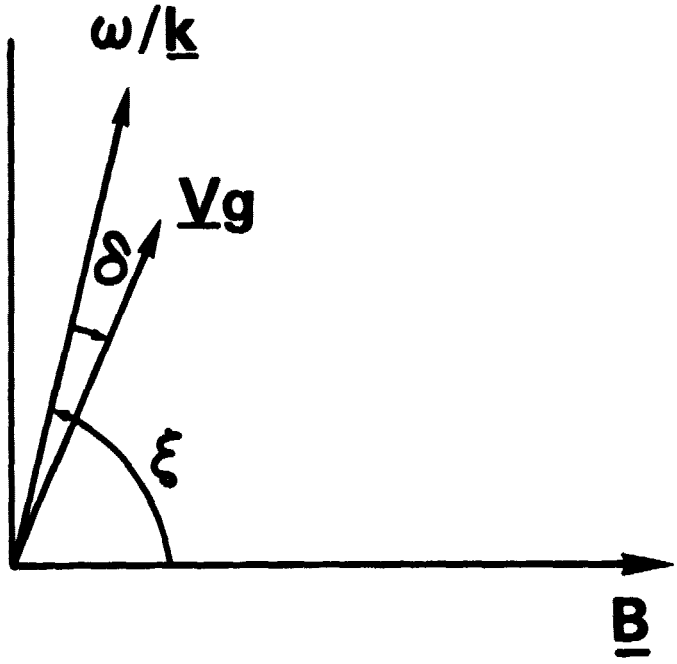

Figure 1. Relationship between $\underset{\sim}{v}_g$, $\omega/\underset{\sim}{k}$ and $\underset{\sim}{B}$. Note that when the Appleton-Hartree dispersion relation is used, δ is negative for the extraordinary mode in Band III.

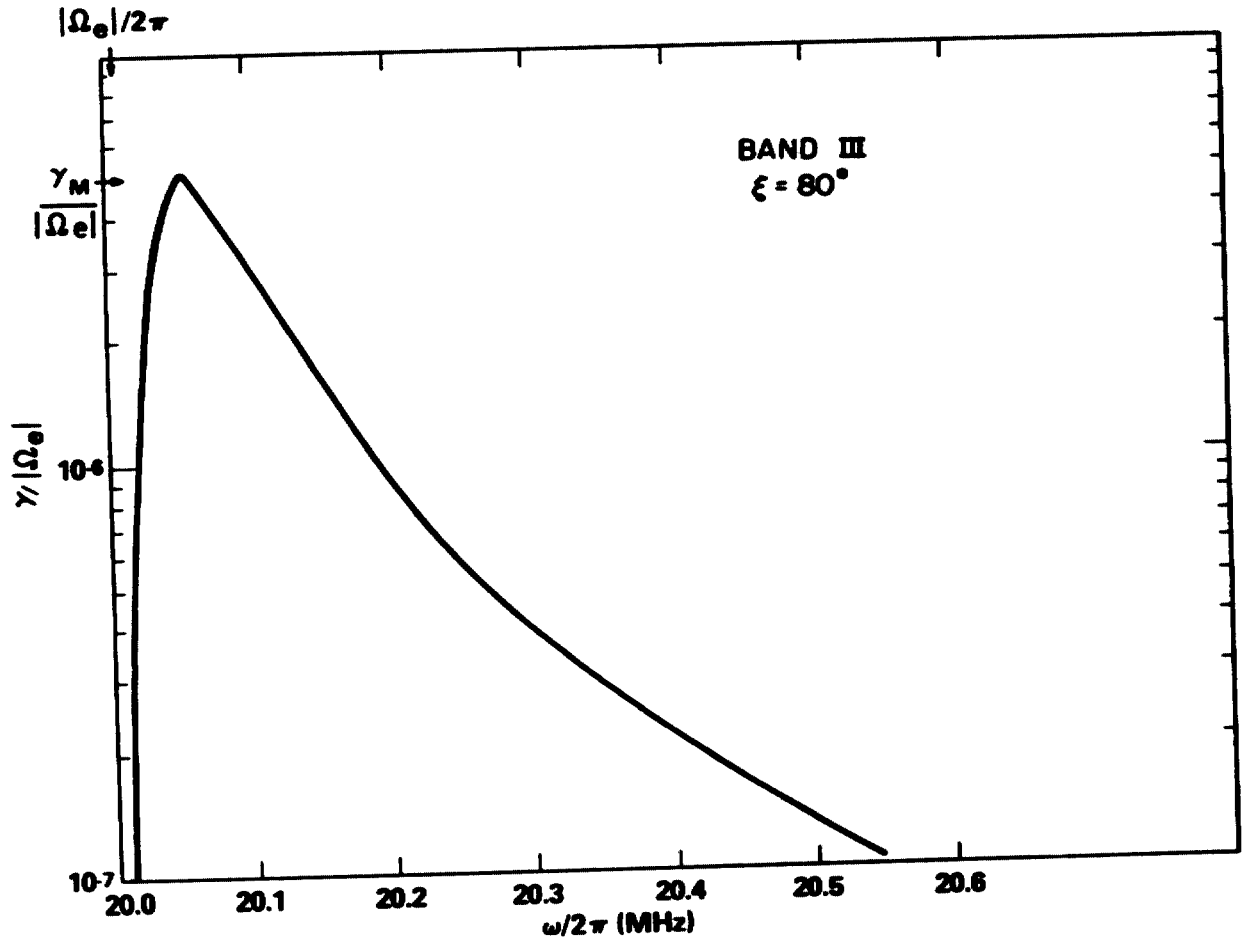

Figure 2. Growth rate versus frequency in Band III. In this calcualtion m = 2, N = 100, $\zeta = 0.1$ and $u_L = 5.9 \times 10^8$ cm s^{-1}. $\underset{\sim}{B}$ was evaluated at r = 1.06 R_{2L}, $\theta = 54°$ north latitude, and $\lambda_{III} = 201.7°$ with the O_4 model. At that point $\alpha_L = 56°$ compared to $\alpha_E = 2.5°$ at the magnetic equator.

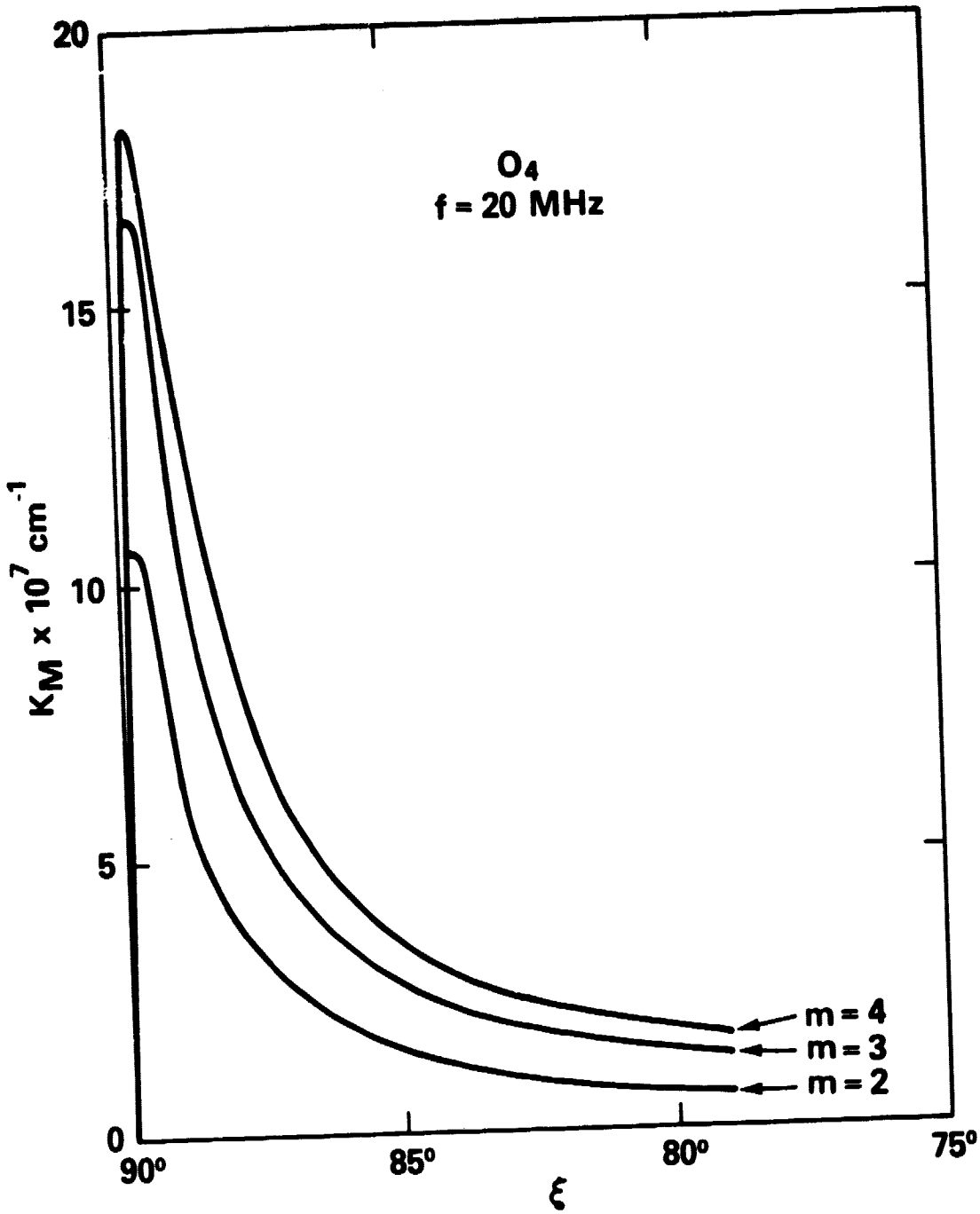

Figure 3. Variation of K_M with ξ for several values of the power-law index, m. N, ζ and u_L as well as r, θ, and λ_{III} are the same as in Figure 2.

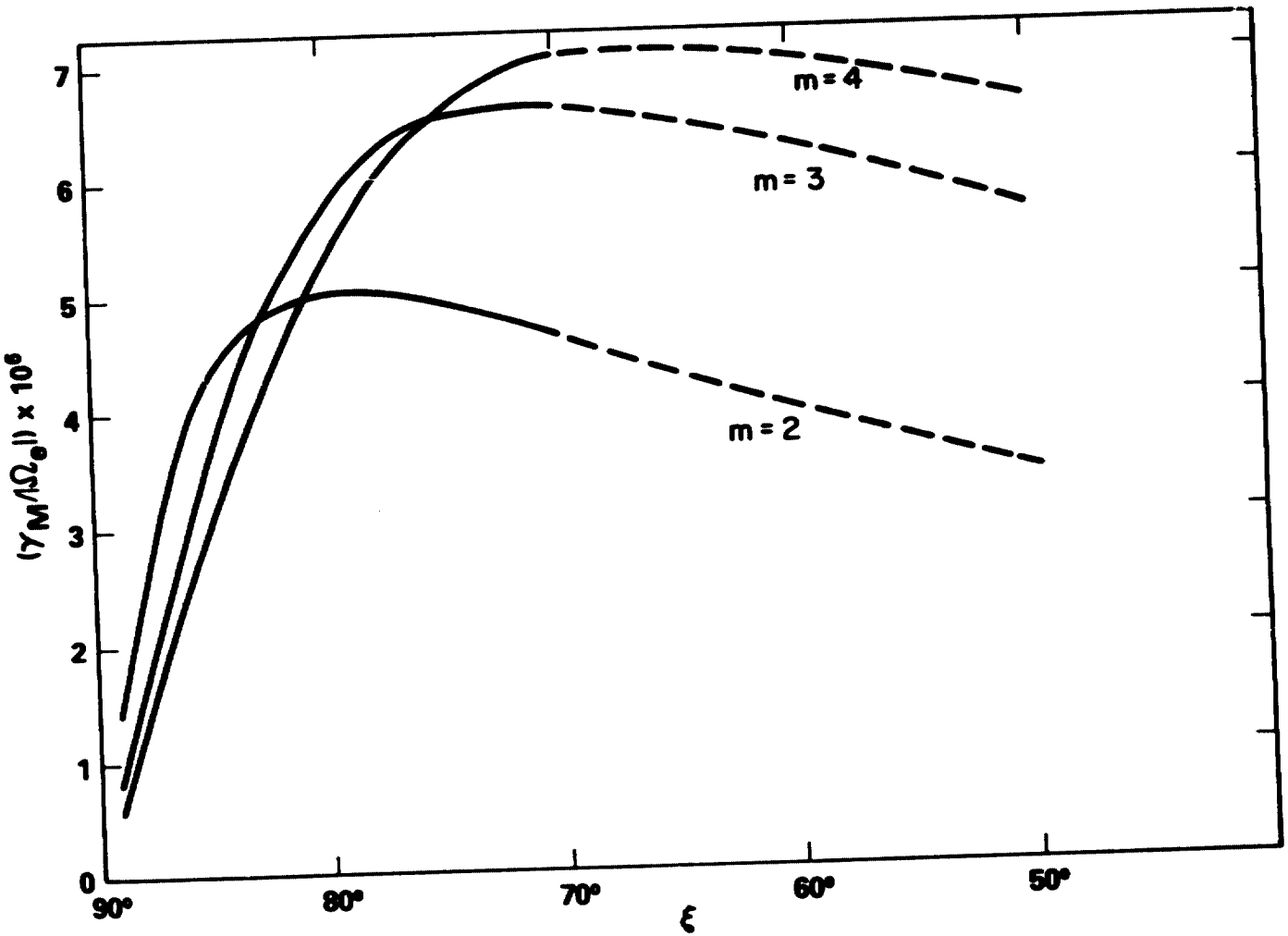

Figure 4. Variation of $\gamma_M/|\Omega_e|$ with ξ for several values of m. Other parameters are the same as in Figure 2.

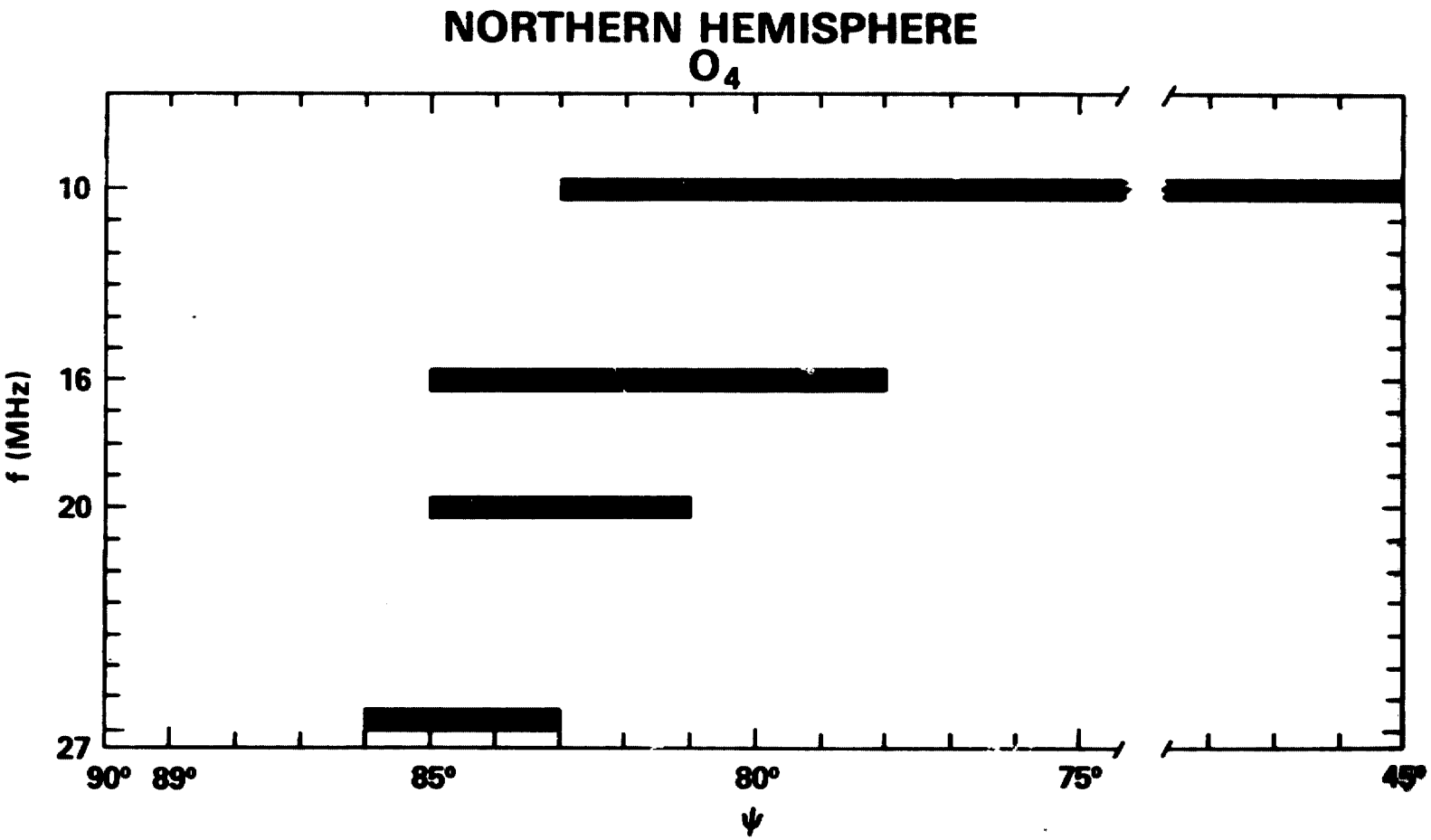

Figure 5. Estimated variation of Ψ with frequency. The limit for large angles is determined by refraction. The cutoff toward small angles indicates when convective amplification is small because the wave has moved out of resonance with the electrons.

ORIGINAL PAGE IS
OF POOR QUALITY

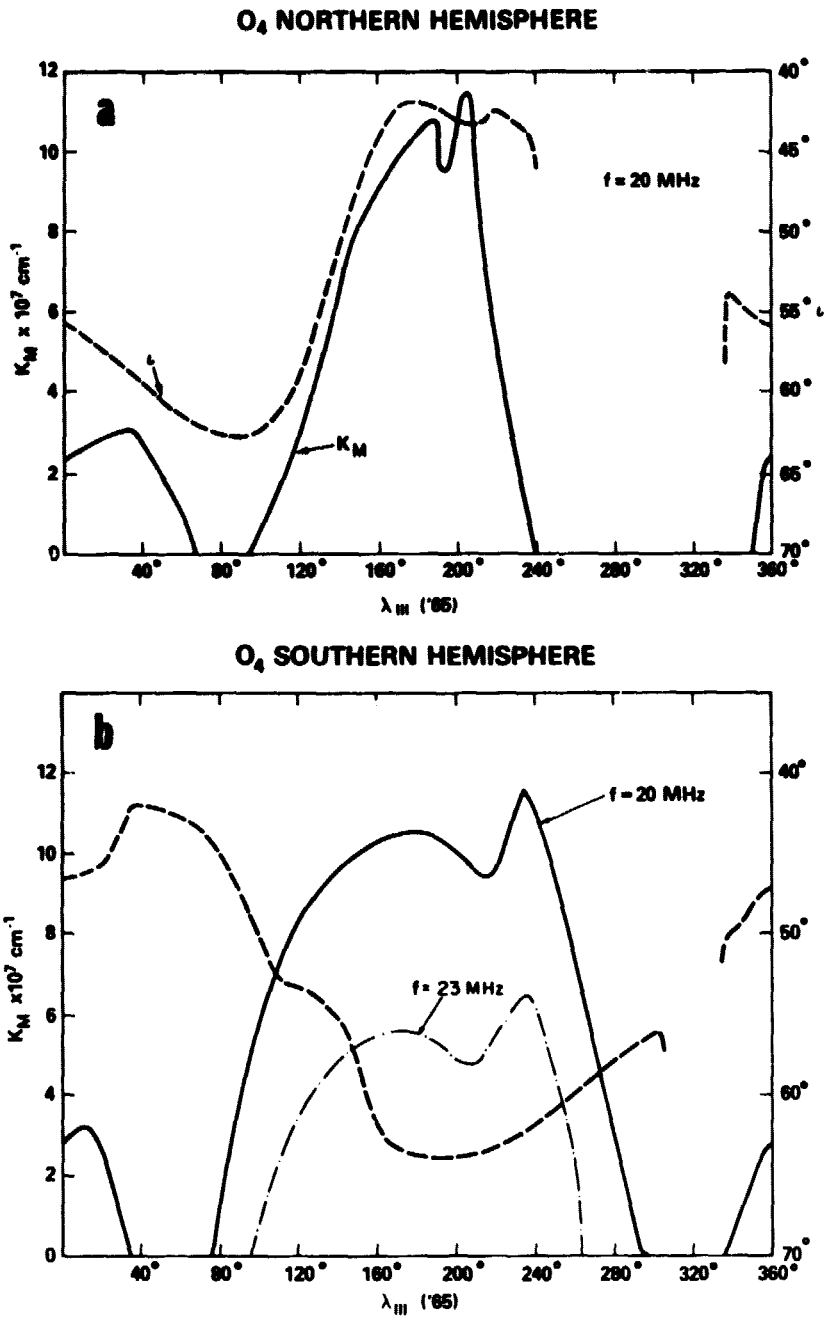

Figure 6. A plot of K_M and ι versus λ_{III} in the northern (a) and southern (b) hemispheres using the O_4 magnetic field model. Note that K_M is large in the northern hemisphere where ι is small. In the southern hemisphere K_M is large where ι is large. Note that in the southern hemisphere ι is plotted for the 20 MHz source height, while K_M is given for both 20 and 23 MHz.

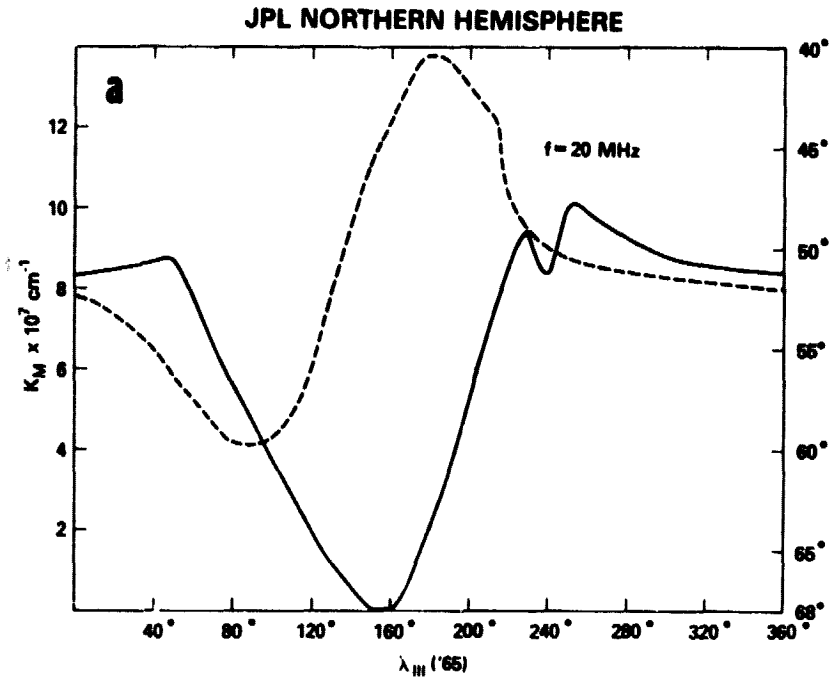

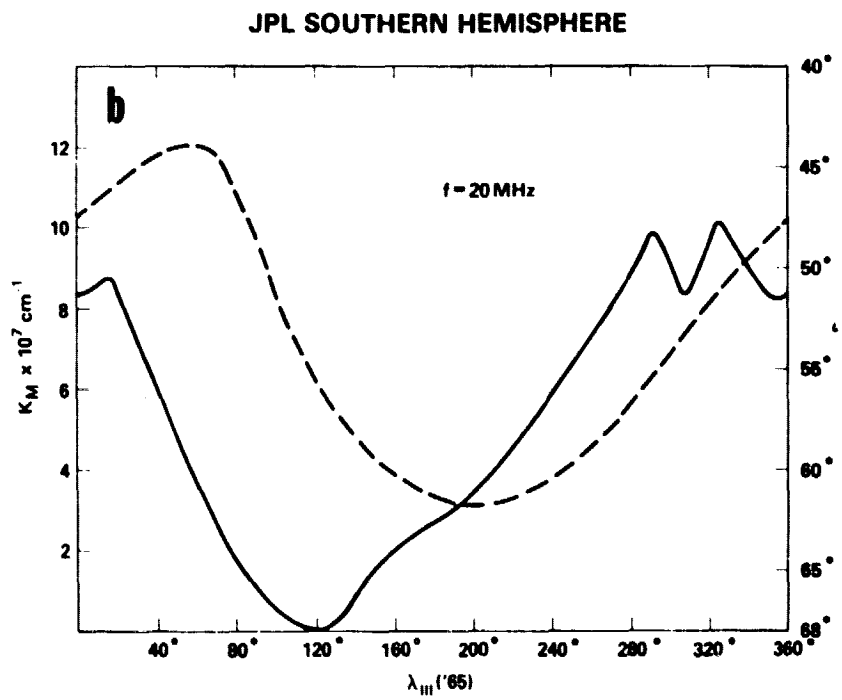

Figure 7. Similar to Figure 6, but using the JPL magnetic field model. Note that ι and K_M are not well correlated in either hemisphere.

ORIGINAL PAGE IS
OF POOR QUALITY

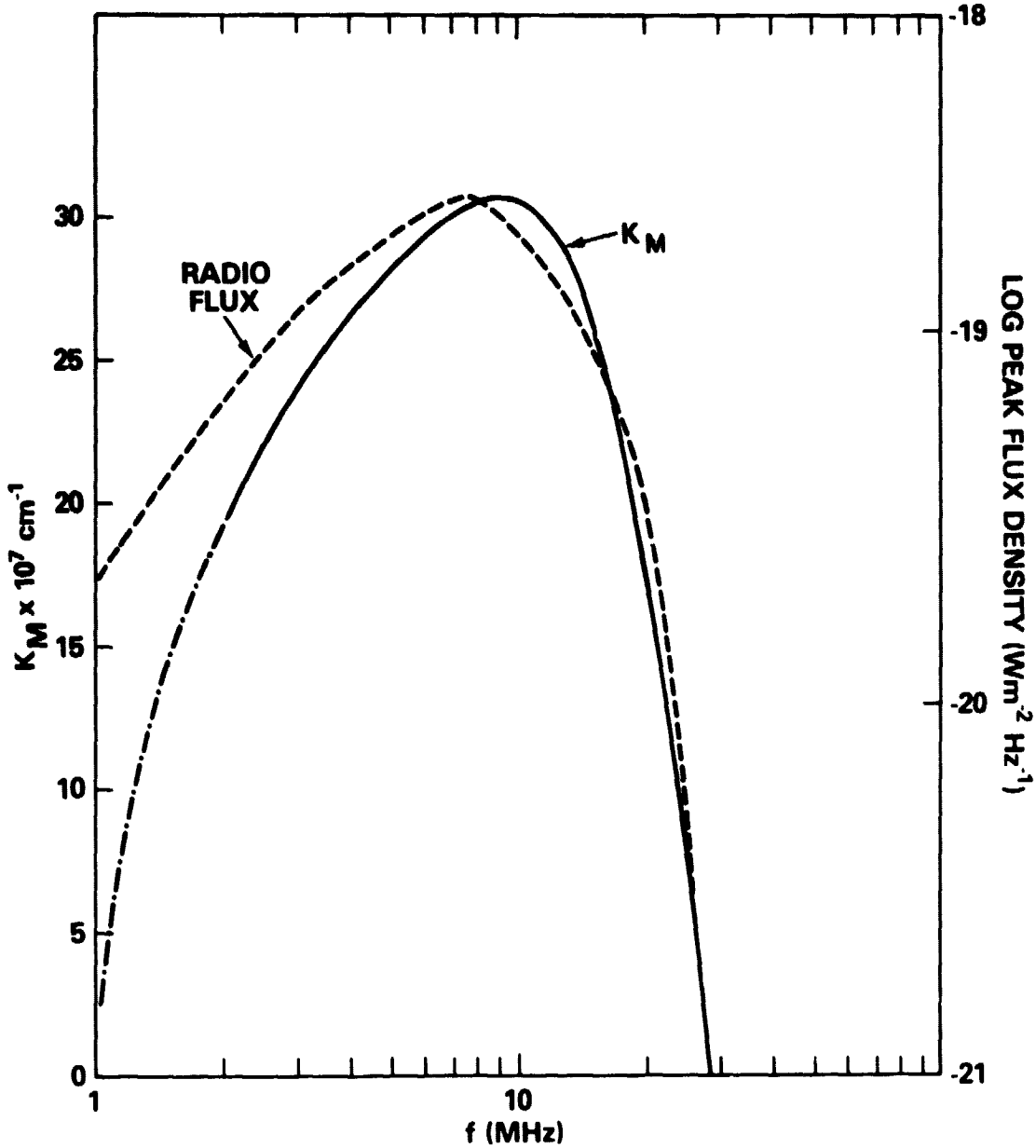

Figure 8. Peak radio flux and K_M plotted against frequency. The radio data is taken from Carr and Desch (1976). K_M is the largest value of $K_M(\xi)$ at each frequency. The shape of the K_M curve is a consequence of using a loss-cone distribution to excite DAM.

TABLES

1 Comparison of observed and predicted source locations using both the O_4 and JPL multipole magnetic field models.

ILLUSTRATIONS

1 Relationship between $\underset{\sim}{v}_g$, $\omega/\underset{\sim}{k}$ and $\underset{\sim}{B}$. Note that when the Appleton-Hartree dispersion relation is used, δ is negative for the extraordinary mode in Band III.

2 Growth rate versus frequency in Band III. In this calculation m = 2, N = 100, ζ = 0.1 and $u_L = 5.9 \times 10^8$ cm s^{-1}. $\underset{\sim}{B}$ was evaluated at r = 1.06 R_{2L}, θ = 54° north latitude, and λ_{III} = 201.7° with the O_4 model. At that point α_L = 56° compared to α_E = 2.5° at the magnetic equator.

3 Variation of K_M with ξ for several values of the power-law index, m. N, ζ and u_L as well as r, θ, and λ_{III} are the same as in Figure 2.

4 Variation of $\gamma_M/|\Omega_e|$ with ξ for several values of m. Other parameters are the same as in Figure 2.

5 Estimated variation of Ψ with frequency. The limit for large angles is determined by refraction. The cutoff toward small angles indicates when convective amplification is small because the wave has moved out of resonance with the electrons.

6 A plot of K_M and ι versus λ_{III} in the northern (a) and southern (b) hemispheres using the O_4 magnetic field model. Note that K_M is large in the northern hemisphere where ι is small. In the southern hemisphere K_M is large where ι is large. Note that in the southern hemisphere ι is plotted for the 20 MHz source height, while K_M is given for both 20 and 23 MHz.

7 Similar to Figure 6, but using the JPL magnetic field model. Note that ι and K_M are not well correlated in either hemisphere.

8 Peak radio flux and K_M plotted against frequency. The radio data is taken from Carr and Desch (1976). K_M is the largest value of $K_M(\xi)$ at each frequency. The shape of the K_M curve is a consequence of using a loss-cone distribution to excite DAM.

BIBLIOGRAPHIC DATA SHEET

1. Report No.	2. Government Accession No.	3. Recipient's Catalog No.
TM 79586		

4. Title and Subtitle	5. Report Date
An Emission Mechanism for the Io-Independent Jovian Decameter Radiation	July 1978
	6. Performing Organization Code
7. Author(s)	8. Performing Organization Report No.
Melvyn L. Goldstein and Aharon Eviatar	
9. Performing Organization Name and Address	10. Work Unit No.
NASA/GSFC Laboratory for Extraterrestrial Physics Interplanetary Physics Branch, Code 692 Greenbelt, MD 20771	11. Contract or Grant No.
	13. Type of Report and Period Covered
12. Sponsoring Agency Name and Address	Technical Memorandum
	14. Sponsoring Agency Code

15. Supplementary Notes

16. Abstract

A theory of the Io-independent decameter radiation is developed. The radiation results from excitation of the electromagnetic loss-cone instability by keV electrons, stably trapped near L = 6. The radiation is excited in Band III of the extraordinary mode. When the effects of refraction are estimated, it is shown that above 10 MHz radiation is beamed into the equatorial plane in a wide, but thin, conical sheet ($\Psi \cong 80^{\circ}$). When the instability analysis is coupled with one of the octupole models of the Jovian magnetic field, the maximum convective growth of the instability occurs in the directions of the non-Io A, B and C sources. The shape of the peak radio flux frequency spectrum is found to be a consequence of the loss cone shape of the electron distribution function.

17. Key Words (Selected by Author(s))	18. Distribution Statement
Jupiter, Decameter Radiation, Loss-Cone Instability	

19. Security Classif. (of this report)	20. Security Classif. (of this page)	21. No. of Pages	22. Price*